Transverse-modal-instability gain in high power fiber amplifiers: Effect of the perturbation relative phase

Michalis N. Zervas

Citation: APL Photonics **4**, 022802 (2019); doi: 10.1063/1.5050523
View online: https://doi.org/10.1063/1.5050523
View Table of Contents: http://aip.scitation.org/toc/app/4/2
Published by the American Institute of Physics

Transverse-modal-instability gain in high power fiber amplifiers: Effect of the perturbation relative phase

Cite as: APL Photonics 4, 022802 (2019); doi: 10.1063/1.5050523
Submitted: 31 July 2018 • Accepted: 25 September 2018 •
Published Online: 11 December 2018

Michalis N. Zervas[a)]

AFFILIATIONS

Optoelectronics Research Centre, University of Southampton, SO17 1BJ Southampton, United Kingdom and Advanced Laser Lab, ORC/SPI Lasers, University of Southampton, SO17 1BJ Southampton, United Kingdom

[a)]Author to whom correspondence should be addressed: mnz@soton.ac.uk

ABSTRACT

Local transverse modal instability (TMI) gain has been derived by carrying out a stability analysis of the fundamental mode amplification in high power fiber amplifiers, in the presence of spatial (transverse) and temporal perturbations, taking into account the gain saturation and resulting thermal loading. We have shown that the relative phase between the fundamental fiber mode and the transverse perturbation significantly affects the local TMI gain. By controlling the relative phase, the TMI gain can be reduced significantly, with the gain variation being more pronounced as the core diameter increases. This finding can be used in conjunction with other proposed approaches to develop efficient strategies for mitigating TMI in high power fiber amplifiers and lasers.

INTRODUCTION

High power fiber lasers (HPFLs) combine a number of unique attributes, such as record output power with close to diffraction limited beam quality, record wall-plug efficiencies, wavelength agility, instant turn-on characteristics, and minimum footprint.[1,2] Such a unique combination of features set them apart from competing laser technologies and have enabled HPFL to aggressively penetrate material processing and other advanced industrial applications.[2–4] In addition, they naturally offer themselves to coherent combination techniques and output power scaling, suitable for the demanding defense applications.[2,4,5]

Further power scaling in single-mode HPFLs has recently been hindered by a new nonlinear effect, namely, transverse modal instability (TMI).[6–20] TMI in high power lasers and amplifiers amounts to a sudden, threshold-like output beam fluctuation and beam quality deterioration above a certain power level. This threshold can be particularly low when large core diameter amplifying fibers are used, such as in the case of high peak power applications.[6]

In high average power operation, the origin of this effect is predominantly thermal and a number of theoretical models have been introduced to explore the nature and investigate the characteristics of TMI. Theoretical models so far have considered the interaction of two propagating modes and studied the power exchange between the modes and TMI threshold through either Stimulated Thermal Rayleigh Scattering (STRS) static or dynamic mode interactions.[6–12] It has also been shown that at small core diameters (<15 μm) and low output powers (<100 W), TMI is attributed predominantly to population inversion effects.[15,16] In an alternative approach, TMI has been studied by considering the stability of the amplified fiber fundamental mode (FM) in the presence of transverse perturbations.[17,18] TMI, along with stimulated Raman scattering (SRS), pump brightness, and bend-induced mechanical reliability, is shown to be limiting the power scalability in high power fiber lasers.[19,20]

The TMI power threshold is influenced by a number of fiber and laser system parameters, such as core/cladding diameter,[18,21] dopant confinement,[22] higher-order mode (HOM) differential losses,[23–25] photodarkening,[26] choice of pump wavelength,[24,27] pumping direction,[25] input signal level, and gain saturation.[28,18] In addition, TMI power threshold is affected significantly by the seed coherence properties and linewidth.[15,29] This dependence is more severe for larger core diameters.[18]

In all previous theoretical studies of TMI gain, only the HOM power exchange has been considered due to the presence of the thermally induced, transversally inhomogeneous refractive-index long-period gratings (RI LPG), following the FM/HOM interference pattern. It has been pointed out that efficient power transfer between the FM and HOM requires a spatial (longitudinal) shift between the FM/HOM interference pattern and the RI LPG. For this to be achieved, a small optical frequency shift (in the kHz range) between FM and HOM has been considered, which results in a traveling interference pattern.[7] When signal phase noise is considered, explicitly on the other hand, it has been shown that it has no impact on the TMI gain.[10]

In addition, a number of experimental techniques have been demonstrated for increasing the TMI threshold in high power fiber amplifiers. They include input signal dithering[30] and pump power modulation[31–33] in order to smear-out thermally generated index gratings. Lately, it has been shown that in the case of pump modulation, the TMI threshold shows a much more complex dependence on pump power and can actually be much lower than the CW case, indicating that relative shifts between the FM/HOM interference pattern and the RI LPG can play a significant role in defining the onset of TMI.[33] In an alternative approach, optical fiber lanterns have been used to apply appropriate phase shifts into and/or to control the amount of excited HOMs at the fiber amplifier input and have been proposed as a technique to mitigate TMI in HPFLs.[36,37]

However, the impact of the relative phase between the amplified FM and the HOM perturbation on the TMI gain has generally been ignored so far. In this paper, we show theoretically that, in addition to the aforementioned fiber and signal parameters, the local TMI gain is affected by differential phase shifts between the amplified FM and the HOM perturbation. Depending on the size and relative sign of the differential phase shifts, the local TMI gain can be increased or substantially decreased. The impact of differential phase shifts is shown to be more pronounced in larger core diameter amplifiers. These new findings throw new light into recent experimental results[30–37] and can be potentially used to develop new strategies for mitigating TMI in HPFLs, improve control algorithms, or devise more efficient launching schemes.

THEORETICAL MODEL OUTLINE

The present TMI approach is based on the stability analysis of the FM (LP_{01}) steady-state amplification, in the presence of steady-state heat load and gain saturation.[18] We consider the electric field of the FM, $E = E_s(r, \varphi, z; t)\exp[i(\beta_s - \omega_0 t)]$, where β_s is the propagation constant and ω_0 is the angular frequency. The paraxial wave equation under the slowly varying envelope approximation, accounting for the effects of the population inversion and thermal load, takes the following form:

$$\frac{\partial E_s}{\partial z} + \frac{1}{v_g}\frac{\partial E_s}{\partial t} - \frac{i}{2\beta_s}\left\{\nabla_T^2 + \left[n_0^2 k_0^2 - \beta_s^2\right]\right\}E_s = \frac{i}{2\beta_s}\omega_0^2\mu_0 P_{NL}, \quad (1)$$

where v_g is the group velocity, n_0 is the core refractive index, and $k_0 = 2\pi/\lambda_0$. $P_{NL} = \varepsilon_0\,\Delta\varepsilon_{NL}\,E_s$ is the nonlinear material polarization and $\Delta\varepsilon_{NL} \approx 2\,n_0\,\Delta n_{NL}$. ∇_T^2 is the transverse Laplacian operator. The nonlinear refractive index Δn_{NL} is given by $\Delta n_{NL} = \Delta n_T + \Delta n_N$, with the refractive index changes due to thermal loading and population inversion given, respectively, by

$$\Delta n_T(r, \varphi, z; t) = (dn/dT)\Delta T(r, \varphi, z; t), \quad (2)$$

$$\Delta n_N(r, \varphi, z; t) = -\frac{i}{2k_0}\left[\left(\sigma_{ap} + \sigma_{ep}\right)(1 + ia)N_2(r, \varphi, z; t) - \sigma_{ap}N_0(r, \varphi, z; t)\right], \quad (3)$$

where ΔT is the core temperature change, (dn/dT) is the thermo-optic coefficient, N_2 is the excited-state population of Yb^{3+}, N_0 is the total Yb^{3+} concentration, σ_{es} (σ_{as}) is the signal emission (absorption) cross section, and a is the ratio of the real and imaginary parts of susceptibility.[15,38]

The variation of the excited state population $N_2(r, \varphi, z; t)$ is described by

$$\frac{dN_2}{dt} = -\frac{N_2}{\tau} - \left[\left(\sigma_{ap} + \sigma_{ep}\right)N_2 - \sigma_{ap}N_0\right]\Phi_p - \left[(\sigma_{as} + \sigma_{es})N_2 - \sigma_{as}N_0\right]\Phi_s, \quad (4)$$

where $\Phi_p(r, \varphi, z; t) = I_p(r, \varphi, z; t)/\left(h\nu_p\right)$ and $\Phi_s(r, \varphi, z; t) = I_s(r, \varphi, z; t)/(h\nu_s)$ are the pump and signal photon fluence distributions, τ is the upper level lifetime, and $I_{p(s)}$ is the pump (signal) intensity. The temperature change distribution $\Delta T(r, \varphi, z; t)$ is given by the heat equation

$$\rho_0 C_0 \frac{d\Delta T}{dt} - \kappa_0 \nabla_T^2(\Delta T) = Q_T, \quad (5)$$

where ρ_0, C_0, and κ_0 are the density, specific heat capacity, and thermal conductivity of glass, respectively, and Q_T is the heat power density given by

$$Q_T(r, \varphi, z; t) = q_D \frac{dI_s(r, \varphi, z; t)}{dz} + \alpha_s I_s(r, \varphi, z; t), \quad (6)$$

where $q_D = (\lambda_s/\lambda_p - 1)$ is the quantum defect and α_s is the signal background loss (including the effect of photodarkening when present). The signal intensity I_s is approximated by $I_s = (n_0/2Z_0)E_{s0}^{-2}$, where E_{s0} is the field amplitude and $Z_0 = 377\ \Omega$ is the impedance of free space.

Next, we follow a standard stability analysis procedure. First, the steady-state amplifier performance for the fundamental mode (LP_{01}) is derived by setting the time derivatives in Eqs. (1), (4), and (5) to zero. Second, the steady-state solutions for the electric field (E_{ss}), upper-state population (N_{2ss}), and temperature distribution (ΔT_{ss}) are perturbed by an infinitesimal amount, as

$$[E_s\ N_2\ \Delta T]^T(r,\varphi,z;t) = [E_{ss} + \varepsilon\ N_{2ss} + \delta n_2\ \Delta T_{ss} + \delta T_0]^T(r,\varphi,z;t), \tag{7}$$

where $[\ldots]^T$ denotes the transpose of $[\ldots]$. All parameters are functions of (r, φ, z; t). The resulted linearized differential equations are further analyzed by considering the Fourier-Hankel transforms of the spatio-temporal perturbations of the electric field $\varepsilon(r, \varphi, z; t)$, upper state population $\delta n_2(r, \varphi, z; t)$, and temperature change $\delta T_0(r, \varphi, z; t)$ expressed as

$$[\varepsilon\ \delta n_2\ \delta T_0]^T(r,\varphi,z;t) = F_m(r,\varphi)\int \left[\tilde{\varepsilon}\ \delta\tilde{n}_2\ \delta\tilde{T}\right]^T(z;\Omega)\, e^{-i\Omega t} d\Omega, \tag{8}$$

where $F_m(r,\varphi) = J_m(u_\varepsilon r)\exp(im\varphi)$ is one term of the Hankel series, expressing transverse harmonics in cylindrical coordinates. $J_m(x)$ are the Bessel functions of 1st kind, and u_ε is the transverse wavenumber of the dominant induced perturbation. In an optical fiber, transverse distributions are discrete, corresponding to supported modes, and the Hankel transform reduces to Hankel series. The RI transverse perturbation harmonics, introduced in this analysis, can be considered as generalized transverse gratings across the fiber core, which scatter light into HOMs. This differentiates the current work from the previous analyses, where power transfer to HOMs is due to the formation of longitudinal RI LPGs. The lowest order RI transverse perturbation component is in the form of the supported LP_{11} mode, which corresponds to a generalized transverse grating of one period.

The electric field perturbation components in Eq. (8) are in general complex numbers, given by $\tilde{\varepsilon}(z;\Omega) = \tilde{\varepsilon}_R(z;\Omega) + i\,\tilde{\varepsilon}_I(z;\Omega) = |\tilde{\varepsilon}(z;\Omega)|\exp[\theta(z;\Omega)]$. $\theta(z;\Omega)$ denotes the relative phase shift distribution between the FM (zeroth order component) and the dominant perturbation component, and its impact on the FM mode amplification stability and TMI gain is the primary scope of this work.

The real and imaginary parts of the electric field perturbation evolution are finally given by

$$\begin{aligned}
\frac{\partial\tilde{\varepsilon}_R}{\partial z} &= +i\frac{\Omega}{v_g}\tilde{\varepsilon}_R - \frac{1}{2}\alpha_\varepsilon\tilde{\varepsilon}_R + \frac{u_T^2}{2\beta_s}\tilde{\varepsilon}_I + \frac{1}{2}(\sigma_{as}+\sigma_{es})E_{ss}\delta\tilde{n}_2,\\
\frac{\partial\tilde{\varepsilon}_I}{\partial z} &= +i\frac{\Omega}{v_g}\tilde{\varepsilon}_I - \frac{1}{2}\alpha_\varepsilon\tilde{\varepsilon}_I - \frac{u_T^2}{2\beta_s}\tilde{\varepsilon}_R + k_0\left(\frac{dn}{dT}\right)E_{ss}\delta\tilde{T}\\
&\quad + \tfrac{1}{2}a(\sigma_{as}+\sigma_{es})E_{ss}\delta\tilde{n}_2,
\end{aligned} \tag{9}$$

where $u_T^2 = u_\varepsilon^2 - u_s^2$ and $u_s^2 = n_0^2k_0^2 - \beta_s^2$. α_ε is the perturbation additional propagation loss. The amplitudes of the transverse inversion and thermal perturbation Fourier components are given by

$$\delta\tilde{n}_2 = -2\frac{P_N}{(\sigma_{as}+\sigma_{es})}\frac{\tilde{\varepsilon}_R}{E_{ss}}; \qquad \delta\tilde{T} = +2P_T I_s\frac{\tilde{\varepsilon}_R}{E_{ss}}, \tag{10}$$

where

$$\begin{aligned}
P_N &= g_s S\frac{1+i\Omega\tau_N}{1+(\Omega\tau_N)^2},\\
P_T &= \frac{1}{\kappa u_\varepsilon^2}\frac{1+i\Omega\tau_T}{1+(\Omega\tau_T)^2}\left\{\alpha_s + \left[q_D g_s\left(1 - S\frac{1+i\Omega\tau_N}{1+(\Omega\tau_N)^2}\right)\right]\right\},
\end{aligned} \tag{11}$$

with $g_s = (\sigma_{es}+\sigma_{as})N_{2ss} - \sigma_{as}N_0$ being the signal saturated gain and $S = (I_s/I_s^{sat})/(1 + I_p/I_p^{sat} + I_s/I_s^{sat})$ being a gain saturation parameter. Substituting Eq. (10) into (9) results in the following system of differential propagation equations for the real and imaginary parts of the electric field,

$$\frac{d}{dz}\begin{bmatrix}\tilde{\varepsilon}_R\\ \tilde{\varepsilon}_I\end{bmatrix} = \begin{bmatrix}M_{11} & M_{12}\\ M_{21} & M_{22}\end{bmatrix}\begin{bmatrix}\tilde{\varepsilon}_R\\ \tilde{\varepsilon}_I\end{bmatrix} \tag{12}$$

with

$$\begin{aligned}
M_{11} &= +i\frac{\Omega}{v_g} - \frac{1}{2}\alpha_\varepsilon - P_N, \quad M_{12} = \frac{u_T^2}{2\beta_s},\\
M_{21} &= -\frac{u_T^2}{2\beta_s} + 2k_0\left(\frac{dn}{dT}\right)P_T I_s - aP_N, \quad M_{22} = +i\frac{\Omega}{v_g} - \frac{1}{2}\alpha_\varepsilon.
\end{aligned} \tag{13}$$

Setting $[\tilde{\varepsilon}_R(z;\Omega)\ \tilde{\varepsilon}_I(z;\Omega)]^T = [\varepsilon_R(\Omega)\ \varepsilon_I(\Omega)]^T\exp(Kz)$ into Eq. (12), we obtain the following two eigenvalues:

$$\begin{aligned}
K_{p(m)} &= +i\frac{\Omega}{v_g} - \frac{1}{2}\alpha_\varepsilon\\
&\quad + \frac{1}{2}\left\{-P_N \pm \sqrt{P_N^2 - 4\frac{u_T^2}{2\beta_s}\left[\frac{u_T^2}{2\beta_s} - 2k_0\left(\frac{dn}{dT}\right)P_T I_s + aP_N\right]}\right\},
\end{aligned} \tag{14}$$

where the subscripts p and m correspond to the (+) and (−) signs, respectively.

TMI power threshold

The TMI threshold is obtained by requiring the argument of the radical (radicant) in Eq. (14) to be greater than zero (radicant >0). In this case, the perturbation experiences substantial additional gain, on top to the one provided by the inversion (given by P_N). In the opposite case (radicant <0), the radical term is imaginary and contributes only to the perturbation phase. The perturbation gain, in the latter case, is only affected by the background loss (α_ε) and the gain term (P_N) due to inversion. In the case of a thermally dominated instability (i.e., when $P_T \gg P_N$), the TMI power threshold is shown to be given by[18]

$$P_{thr} = \frac{\kappa U_\varepsilon^2\left(U_\varepsilon^2 - U_s^2\right)}{16\pi n_{eff}\left(\frac{\partial n}{\partial T}\right)\alpha_s'}\left(\frac{\lambda_s}{R_0}\right)^2, \tag{15}$$

where $\alpha_s' \approx \alpha_s + (1 - S)q_D g_s$. For well-saturated high power amplifiers, $S \approx 0.5$. For $P \geq P_{thr}$, small transverse amplitude and/or phase perturbations grow exponentially and lead to TMI. For $P < P_{thr}$, on the other hand, they die out and the FM amplification is stable. P_{thr} is inversely proportional to the quantum defect (q_D) and the saturated amplifier gain (g_s). It is proportional to $(\lambda_s/R_0)^2$, which is in good agreement with experimental data.[18]

In the case of a step-index fiber, the transverse wavenumbers for the fundamental (LP_{01}) and perturbation (LP_{11}) modes are approximated by[39]

$$U_\varepsilon(V) = U_\varepsilon(\infty)e^{-(1/V)}, \tag{16}$$

where $U_\varepsilon = u_\varepsilon R_0$ is the normalized transverse wavenumber and the asymptotic value $U_\varepsilon(\infty)$ is 2.405 for LP_{01}, 3.832 for LP_{11}, 5.135 for LP_{21}, and 5.520 for LP_{02} modes. $V = k_0\ R_0\ NA$ is the fiber normalized frequency, NA is the core numerical aperture, and r_0 is the core radius.

Local TMI gain

The local TMI gain can be obtained analytically by assuming that the signal and pump powers are constant over a segment ΔL. An appropriate length is comparable to the seed coherence length. For a seed linewidth of ~20 GHz, the corresponding coherence length is $L_c \approx 1$ cm.

The local TMI gain can be calculated by the solution of propagation [Eq. (12)]. For fixed signal and pump powers, parameters M_{ij} ($i, j = 1, 2$) are constant and the real and imaginary parts of the transverse perturbation at the output of a segment ΔL are then given by

$$\begin{bmatrix}\tilde{\varepsilon}_R(\Delta L;\Omega)\\ \tilde{\varepsilon}_I(\Delta L;\Omega)\end{bmatrix} = c_p\begin{bmatrix}\varepsilon_{1p}\\ \varepsilon_{2p}\end{bmatrix}\exp(K_p\Delta L) + c_m\begin{bmatrix}\varepsilon_{1m}\\ \varepsilon_{2m}\end{bmatrix}\exp(K_m\Delta L), \tag{17}$$

where $[\varepsilon_{1p}\ \varepsilon_{2p}]^T$, $[\varepsilon_{1m}\ \varepsilon_{2m}]^T$ are the corresponding local eigenvectors defining the perturbation local gain as a function of the local signal and pump powers. The eigenvectors are given by $[\varepsilon_{1p(m)}\ \varepsilon_{2p(m)}]^T = [M_{12}/(M_{11} - K_{p(m)})\ 1]^T$. Finally, the constants c_p and c_m are defined by the boundary conditions and depend on the relative phase θ_0 between the FM and the HOM perturbation at the input of the segment ΔL,

$$\tilde{\varepsilon}(0;\Omega) = \tilde{\varepsilon}_{0R}(0;\Omega) + i\,\tilde{\varepsilon}_{0I}(0;\Omega) = |\tilde{\varepsilon}_0(\Omega)|\exp(i\theta_0). \tag{18}$$

The final expressions are

$$\begin{aligned}\tilde{\varepsilon}_R(\Delta L;\Omega) &= c_{p0}\left(\frac{M_{22} - K_p}{M_{21}}\right)\exp(K_p\Delta L)\\ &\quad + c_{m0}\left(\frac{M_{22} - K_m}{M_{21}}\right)\exp(K_m\Delta L),\\ \tilde{\varepsilon}_I(\Delta L;\Omega) &= c_{p0}\exp(K_p\Delta L) + c_{m0}\exp(K_m\Delta L),\end{aligned} \tag{19}$$

where

$$c_{p0} = \frac{-\tilde{\varepsilon}_{0R}M_{21} + \tilde{\varepsilon}_{0I}(M_{22} - K_m)}{(K_p - K_m)},\quad c_{m0} = \frac{+\tilde{\varepsilon}_{0R}M_{21} - \tilde{\varepsilon}_{0I}(M_{22} - K_p)}{(K_p - K_m)}. \tag{20}$$

The local TMI gain G_{TMI} over the segment ΔL is then given by

$$G_{TMI}(\Delta L;\Omega) = \frac{|\tilde{\varepsilon}(\Delta L;\Omega)|^2}{|\tilde{\varepsilon}_0(\Omega)|^2} = \frac{|\tilde{\varepsilon}_R(\Delta L;\Omega)|^2 + |\tilde{\varepsilon}_I(\Delta L;\Omega)|^2}{|\tilde{\varepsilon}_0(\Omega)|^2}. \tag{21}$$

NUMERICAL RESULTS

From the preceding analysis, it is apparent that the local TMI gain depends on the signal power (P_s) and saturated gain (g_s), as well as the perturbation transverse wavenumber (u_ε) and frequency offset with respect to the laser frequency (Ω). For a fixed V number (i.e., fiber modality), the TMI threshold and local gain depend on the core radius, through P_T [Eq. (11)] and Eq. (15). In addition, local TMI gain is expected to depend on the relative phase shift (θ_0) of the perturbation with respect to FM, through constants c_p and c_m [Eq. (20)]. This last TMI gain dependence is largely unexplored so far. Key modeling parameters are summarized in the Appendix (Table I), and they will be used in the calculations, unless otherwise stated.

Figure 1(a) shows the local TMI gain variation with TMI frequency and signal power, for the phase shift between the fundamental mode and the perturbation $\theta_0 = 0\pi$. The core diameter is 60 μm, and the corresponding TMI power threshold, as calculated by Eq. (15), is $P_{thr} = 460$ W. It is shown that the local TMI gain increases sharply for powers larger than the TMI threshold. Figures 1(b) and 1(c) show that the local TMI gain distribution is affected significantly by a variation of the relative phase shift θ_0. It is shown that a positive phase shift [$\theta_0 = +0.3\pi$, Fig. 1(b)] significantly decreases the TMI gain, while a negative phase shift [$\theta_0 = -0.3\pi$; Fig. 1(c)] increases the TMI gain. Figure 1(d) compares the local TMI gain variation with frequency for the aforementioned phase shifts, at a signal power of $P_s = 800$ W. In this case, it is shown that a phase shift of $\theta_0 = -0.3\pi$ results in an ~130% TMI gain increase, while $\theta_0 = +0.3\pi$ results in an ~80% gain decrease.

Figure 2 plots the local TMI gain variation with the perturbation frequency offset (Ω) and relative phase shift (θ_0), for core radii of (a) 10 μm, (b) 20 μm, (c) 30 μm, and (d) 40 μm. The local signal power is $P_s = 1000$ W. It is clearly demonstrated that the local TMI gain is affected to different degrees by the relative phase shift θ_0 for different core radii. For the smaller core radius [$R_0 = 10$ μm, Fig. 2(a)], we observe low local TMI gain and minimal variation with the perturbation phase shift. In addition, TMI gain peaks at relatively large (several kHz) positive frequency offsets and shows a wide effective bandwidth. With larger core radii, the local TMI gain increases and it becomes progressively more "localized," with smaller positive frequency offsets and narrower effective bandwidths. In all cases, the peak local TMI gain occurs for negative perturbation phase shifts. Both the peak TMI gain and the associated frequency offset vary with the perturbation phase shift.

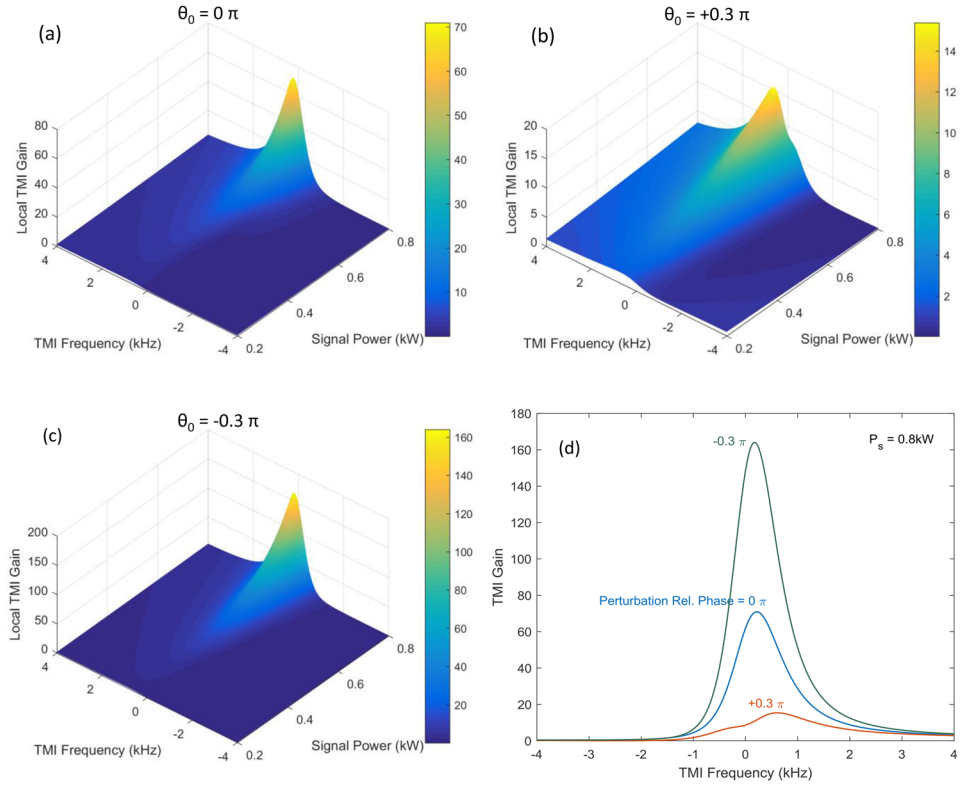

FIG. 1. Local TMI gain variation with TMI frequency (Ω) and signal power for phase shifts (θ_0) between the fundamental mode and the perturbation of (a) 0π, (b) $+0.3\pi$, and (c) -0.3π. (d) Comparison of local TMI gain at signal power P_s = 800 W. Core diameter = 60 μm and P_{thr} = 460 W.

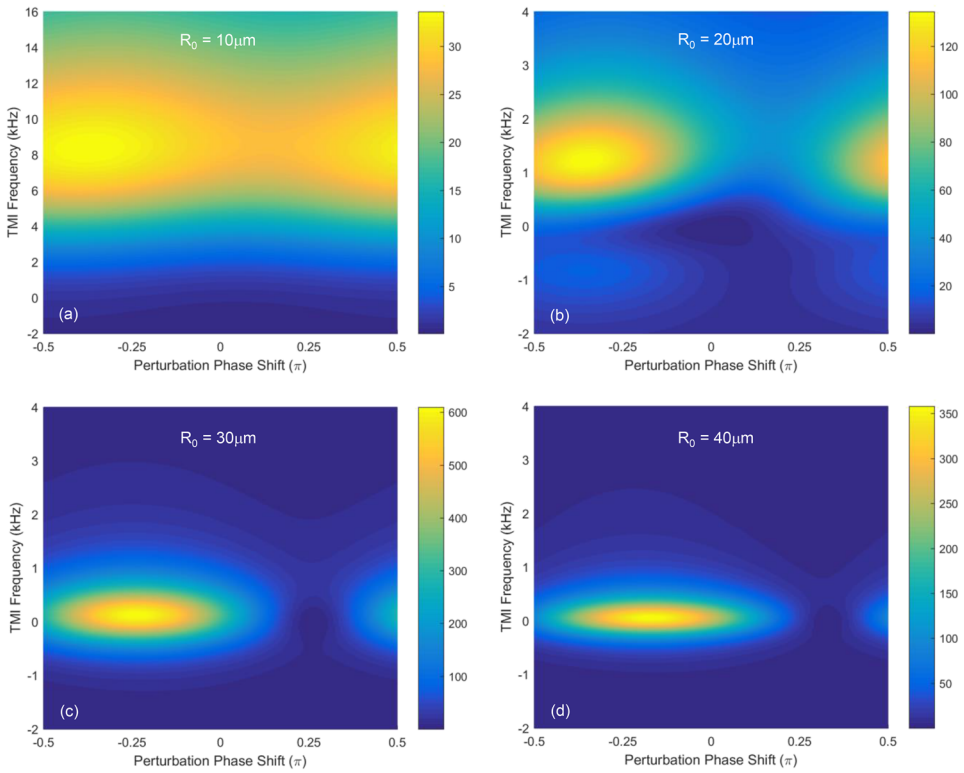

FIG. 2. Local TMI gain variation with perturbation frequency offset (Ω) and relative phase shift (θ_0) for core radii of (a) 10 μm, (b) 20 μm, (c) 30 μm, and (d) 40 μm. Signal power P_s = 1000 W.

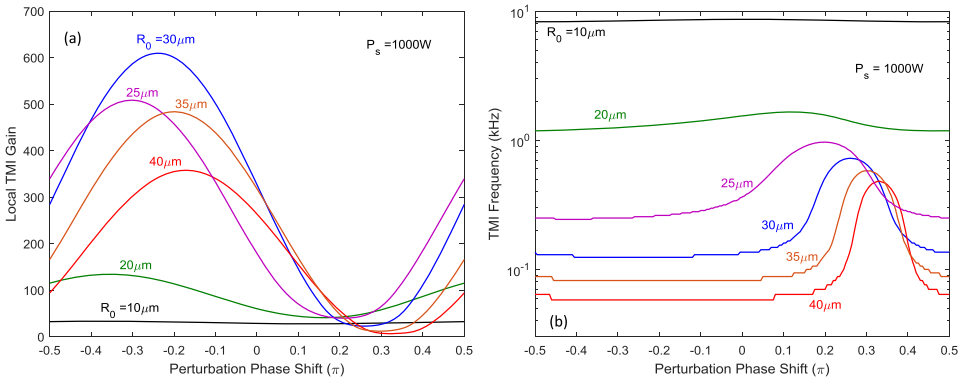

FIG. 3. (a) Peak local TMI gain and (b) associated TMI frequency as a function of the relative perturbation phase shift (θ_0) for different core radii. P_s = 1000 W.

Figure 3 plots (a) the peak local TMI gain and (b) associated TMI frequency as a function of the relative perturbation phase shift (θ_0) for different core radii. The signal power is P_s = 1000 W. It is shown that the impact of the perturbation relative phase shift on the peak TMI gain is more pronounced as the core radius increases. For core radius R_0 = 10 μm, the perturbation relative phase shift has almost no impact on the local TMI gain. As the core diameter increases, the local TMI gain experiences substantial changes. This implies that variation of the perturbation relative phase shift will be more effective in controlling TMI effects in larger core diameter fibers.

The impact of the perturbation relative phase shift on the local TMI gain is further explored by considering its behavior with signal powers around the TMI power threshold. Figure 4 shows (a) the peak local TMI gain and (b) the associated TMI frequency as a function of the perturbation relative phase shift for different signal powers. The core/cladding diameters are 80/250 μm, and the Yb^{3+} dopant concentration is $N_0 = 5 \times 10^{+25}$ m^{-3}. These parameters are in line with the ones used in Refs. 32 and 33. Note that the considered dopant concentration level can vary depending on the actual pump, signal emission, and absorption cross sections, which are known to depend on the core glass material. The nominal TMI power threshold in this case, as calculated by Eq. (15), is P_{thr} = 265 W, which is in very good agreement with the experimental value (233-270 W).[32,33]

It should be mentioned that the nominal TMI power threshold corresponds to $\theta_0 = 0$ and in this case shows a local TMI gain of ~2.5. As shown in Fig. 4, introducing a positive perturbation phase shift in the range $0 < \theta_0 < +0.38\pi$ reduces the local TMI gain and results in an effective TMI threshold increase. Outside this range, the local TMI gain increases and the effective TMI power threshold is expected to decrease. It is also shown that even at signal powers well below the nominal TMI threshold (e.g., P_s = 160 W), there is a range of negative perturbation phase shifts (i.e., $-0.48\pi < \theta_0 < -0.25\pi$), where the local TMI gain increases above the nominal TMI threshold gain and TMI can occur. On the other hand, at signal powers well above the nominal TMI threshold (e.g., P_s = 460 W), there is a range of positive perturbation phase shifts (i.e., $+0.18\pi < \theta_0 < +0.32\pi$), where the local TMI gain decreases below the nominal TMI threshold gain and TMI is not expected to occur. These results demonstrate that, in this case with nominal P_{thr} = 265 W, when the perturbation relative phase shift is (intentionally or unintentionally) varied, the TMI power threshold can vary from ~160 W to ~460 W. As the power is increased in this range, the "TMI-free" perturbation phase shift range decreases. This dependence of the TMI power threshold on the perturbation phase shift is

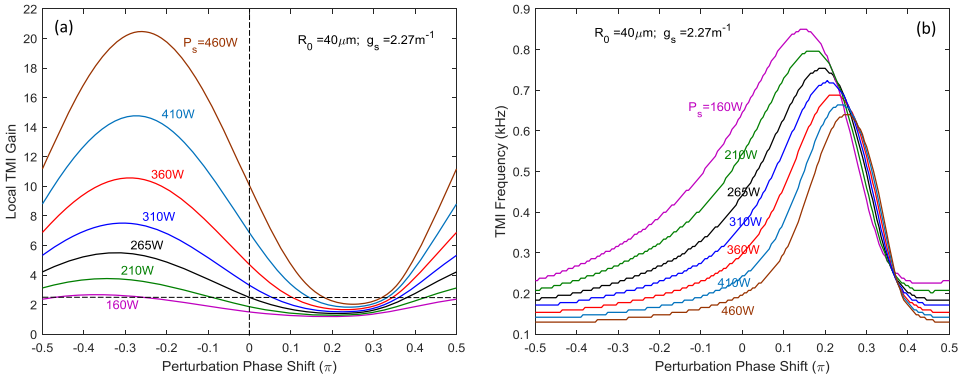

FIG. 4. (a) Peak local TMI gain and (b) associated TMI frequency as a function of the perturbation relative phase shift (θ_0) for different signal powers. The core/cladding diameters are 80/250 μm. Nominal TMI power threshold P_{thr} = 265 W.

in accordance with recent experimental results, where phase shifts are believed to be experimentally introduced by pump modulation.[33,34]

DISCUSSION AND SUMMARY

In this work, we performed a stability analysis of the FM mode amplification in the presence of a transverse perturbation (in the form of a HOM) and derived the TMI gain in the presence of a phase shift between the FM and the induced perturbation (θ_0). In our case, the induced perturbation (generalized RI grating) is transverse in nature (rather than longitudinal, as in all previous studies) and the TMI gain is a result of a transverse scattering of the FM, rather than power exchange due to a longitudinal RI LPG.

We have shown theoretically that in addition to the perturbation frequency offset (Ω), the local TMI gain is impacted by relative phase shifts (θ_0). This impact also depends on the local signal and pump powers, dopant concentration, and core diameter. It is shown that the local TMI gain can be decreased or even increased substantially with respect to the in-phase response. The gain variation is more pronounced as the core diameter increases. This is an important finding, which can be used in conjunction with other proposed approaches to develop efficient strategies for increasing TMI threshold in high power fiber amplifiers and lasers. It can also be used to gain some physical insight into the origin of the observed large differences in the TMI threshold dependence on core diameter for narrow and broad linewidth operation.[18] This phase shift can also be induced externally due to the launching conditions[30,36] or internally due to non-uniform fiber core stresses, heat, or inversion distribution.

The analysis has been applied to short amplifier segments, defined primarily by the degree of seed coherence. It can be extended to full amplifier lengths, where the signal and inversion vary, through a piece-wise approximation and transfer matrix approach. The overall TMI gain and TMI threshold depend on the distributed differential phase shifts, which are affected by the seed coherence properties, and the distributed gain saturation. This study is beyond the scope of this paper.

Similar dependence of the transverse mode instability (called filamentation) gain on the relative perturbation phase has been studied in the context of wide aperture semiconductor amplifiers, where the transverse instability is shown to be dominated merely by inversion effects.[40]

The dependence of high power fiber amplifier TMI gain on the relative perturbation phase can account for the experimental observation of TMI thresholds significantly lower than the CW pumping case when pumps are modulated.[33,34] In this case, although the input residual LP_{11} mode and relative phase shift are to a large extent unchanged, the relative phase shift is changing periodically during each pumping cycle downstream in the counter-pumped amplifier. This work offers an alternative approach to the phase shift development between the signal interference pattern and the longitudinal RI LPG, presented in Ref. 35, to explain the recent experimental results presented in Ref. 34.

ACKNOWLEDGMENTS

The author acknowledges support from the Royal Academy of Engineering under the Research Chairs and Senior Research Fellowships Scheme and also the Engineering and Physical Sciences Research Council (EPSRC) (No. EP/P027644/1). The data can be found at https://doi.org/10.5258/SOTON/D0670.

APPENDIX: MODELING PARAMETERS

TABLE I. Key modeling parameters.

Thermal conductivity (κ_0)	1.4	W/(m K)
Specific heat capacity (C_0)	$0.84 \times 10^{+3}$	J/(Kg K)
Glass density (ρ_0)	$2.2 \times 10^{+3}$	kg/m^{+3}
Thermo-optic coefficient (dn/dT)	1.2×10^{-5}	
Yb^{3+} concentration (N_0)	$1 \times 10^{+26}$	m^{-3}
Metastable level lifetime (τ)	1×10^{-3}	s
Real-to-imaginary susceptibility ratio (a)	10	
Signal wavelength (λ_s)	1064	nm
Signal emission cross section (σ_{es})	0.14×10^{-24}	m^2
Signal absorption cross section (σ_{as})	0.0016×10^{-24}	m^2
Pump wavelength (λ_p)	976	nm
Pump emission cross section (σ_{ep})	1.46×10^{-24}	m^2
Pump absorption cross section (σ_{ap})	1.38×10^{-24}	m^2
Cladding-to-core diameter ratio	6	
Optical-to-optical conversion efficiency (η_{OO})	75%	

REFERENCES

[1] M. N. Zervas and C. A. Codemard, "High power fiber lasers: A review," IEEE J. Sel. Top. Quantum Electron. **20**, 0904123 (2014).

[2] L. Dong and B. Samson, *Fiber Lasers* (CRC Press, Taylor & Francis Group, 2017).

[3] Y. Kawahito, M. Mizutani, and S. Katayama, "High quality welding of stainless steel with 10 kW high power fibre laser," Sci. Technol. Weld. Joining **14**, 288 (2009).

[4] M. O'Connor and B. Shiner, "High power fiber lasers for industry and defence," in *High Power Laser Handbook*, edited by H. Injeyan and G. D. Goodno (McGraw Hill, N.Y., 2011), Chap. 18.

[5] E. Honea, R. S. Afzal, M. Savage-Leuchs, J. Henrie, K. Brar, N. Kurz, D. Jander, N. Gitkind, D. Hu, C. Robin, A. M. Jones, R. Kasinadhuni, and R. Humphreys, "Advances in fiber laser spectral beam combining for power scaling," Proc. SPIE **9730**, 97300Y (2016).

[6] T. Eidam, C. Wirth, C. Jauregui, F. Stutzki, F. Jansen, H.-J. Otto, O. Schmidt, T. Schreiber, J. Limpert, and A. Tunnermann, "Experimental observations of the threshold-like onset of mode instabilities in high power fiber amplifiers," Opt. Express **19**, 13218 (2011).

[7] A. V. Smith and J. J. Smith, "Mode instability in high power fiber amplifiers," Opt. Express **19**, 10180 (2011).

[8] C. Jauregui, T. Eidam, H.-J. Otto, F. Stutzki, F. Jansen, J. Limpert, and A. Tunnermann, "Physical origin of mode instabilities in high power fiber laser systems," Opt. Express **20**, 12912 (2012).

[9] A. V. Smith and J. J. Smith, "Steady-periodic method for modelling mode instability in fiber amplifiers," Opt. Express **21**, 2606–2623 (2013).

[10] K. R. Hansen, T. T. Alkeskjold, J. Broeng, and J. Lægsgaard, "Theoretical analysis of mode instability in high-power fiber amplifiers," Opt. Express **21**, 1944 (2013).

[11] L. Dong, "Stimulated thermal Rayleigh scattering in optical fibers," Opt. Express **21**, 2642 (2013).

[12] S. Naderi, I. Dajani, T. Madden, and C. Robin, "Investigations of modal instabilities in fiber amplifiers through detailed numerical simulations," Opt. Express **21**, 16111 (2013).

[13] B. G. Ward, "Modeling of transient modal instability in fiber amplifiers," Opt. Express **21**, 12053 (2013).

[14] R. Tao, P. Ma, X. Wang, P. Zhou, and Z. Liu, "1.3 kW monolithic linearly polarized single-mode master oscillator power amplifier and strategies for mitigating mode instabilities," Photonics Res. **3**, 86 (2015).

[15] M. Kuznetsov, O. Vershinin, V. Tyrtyshnyy, and O. Antipov, "Low-threshold mode instability in Yb^{3+}-doped few-mode fiber amplifiers," Opt. Express **22**, 29714 (2014).

[16] D. Alekseev, V. Tyrtyshnyy, M. Kuznetsov, and O. Antipov, "Transverse-mode instability in high-gain few-mode Yb^{3+}-doped fiber amplifiers with a 10-μm core diameter with or without backward reflection," IEEE J. Sel. Top. Quantum Electron. **24**, 5100608 (2018).

[17] M. N. Zervas, "TMI threshold in high power fiber amplifiers," in OSA Advanced Photonics Congress, 2016, SoW2H.2.

[18] M. N. Zervas, "Transverse mode instability analysis in fiber amplifiers," Proc. SPIE **10083**, 100830M (2017).

[19] M. N. Zervas, "Power scalability in high power fiber amplifiers," in CLEO/Europe-EQEC, 2017, paper CJ-6.1.

[20] M. N. Zervas, "Power scaling limits in high power fiber amplifiers due to transverse mode instability, thermal lensing and fiber mechanical reliability," Proc. SPIE **10512**, 1051205 (2018).

[21] A. V. Smith and J. J. Smith, "Raising the mode instability thresholds in fiber amplifiers," Proc. SPIE **8961**, 89611S (2014).

[22] C. Robin, I. Dajani, C. Zeringue, B. Ward, and A. Lanari, "Gain-tailored SBS suppressing photonic crystal fibers for high power applications," Proc. SPIE **8237**, 82371D (2012).

[23] M. Laurila, M. M. Jørgensen, K. R. Hansen, T. T. Alkeskjold, J. Broeng, and J. Lægsgaard, "Distributed mode filtering rod fiber amplifier delivering 292W with improved mode stability," Opt. Express **20**, 5742 (2012).

[24] K. Hejaz, A. Norouzey, R. Poozesh, A. Heidariazar, A. Roohforouz, R. Rezaei Nasirabad, N. Tabatabaei Jafari, A. Hamedani Golshan, A. Babazadeh, and M. Lafouti, "Controlling mode instability in a 500 W ytterbium-doped fiber laser," Laser Phys. **24**, 025102 (2014).

[25] C. X. Yu, O. Shatrovoy, T. Y. Fan, and T. F. Taunay, "Diode-pumped narrow linewidth multi-kilowatt metalized Yb fiber amplifier," Opt. Lett. **41**, 5202 (2016).

[26] H.-J. Otto, N. Modsching, C. Jauregui, J. Limpert, and A. Tünnermann, "The impact of photodarkening on the mode instability threshold," Opt. Express **23**, 15265 (2015).

[27] K. Brar, M. Savage-Leuchs, J. Henrie, S. Courtney, C. Dilley, R. Afzal, and E. Honea, "Threshold power and fiber degradation induced modal instabilities in high power fiber amplifiers based on large mode area fibers," Proc. SPIE **8961**, 89611R (2014).

[28] A. V. Smith and J. J. Smith, "Increased mode instability thresholds by gain saturation," Opt. Express **21**, 15168 (2013).

[29] J. J. Smith and A. V. Smith, "Influence of signal bandwidth on mode instability thresholds of fiber amplifiers," Proc. SPIE **9344**, 93440L (2015).

[30] H. J. Otto, C. Jauregui, F. Stutzki, F. Jansen, J. Limpert, and A. Tünnermann, "Controlling mode instabilities by dynamic mode excitation with an acousto-optic deflector," Opt. Express **21**, 17285 (2013).

[31] C. Stihler, C. Jauregui, H.-J. Otto, J. Limpert, and A. Tünnermann, "Controlling mode instabilities at 628 W average output power in an Yb-doped rod-type fiber amplifier by active modulation of the pump power," Proc. SPIE **10083**, 100830P (2017).

[32] C. Jauregui, C. Stihler, J. Limpert, and A. Tünnermann, "Pump-modulation-induced beam stabilization in high-power fiber laser systems above the mode instability threshold," Opt. Express **26**, 10691 (2018).

[33] C. Stihler, C. Jauregui, J. Limpert, and A. Tünnermann, "Towards the control of the modal energy transfer in transverse mode instabilities," Proc. SPIE **10512**, 1051204 (2018).

[34] C. Stihler, C. Jauregui, A. Tünnermann, and J. Limpert, "Modal energy transfer by thermally induced refractive index gratings in Yb-doped fibers," Light: Sci. Appl. **7**, 59 (2018).

[35] C. Stihler, C. Jauregui, A. Tünnermann, and J. Limpert, "Phase-shift evolution between the modal interference pattern and the thermally-induced refractive index grating in high-power fiber laser systems," Opt. Express **26**, 19489–19497 (2018).

[36] J. Montoya, C. Aleshire, C. Hwang, N. K. Fontaine, A. Velázquez-Benítez, D. H. Martz, T. Y. Fan, and D. Ripin, "Photonic lantern adaptive spatial mode control in LMA fiber amplifiers," Opt. Express **24**, 3405 (2016).

[37] J. Montoya, C. Hwang, D. H. Martz, C. Aleshire, T. Y. Fan, and D. Ripin, "Photonic lantern kW-class fiber amplifier," Opt. Express **25**, 27543 (2017).

[38] A. Fotiadi, O. Antipov, M. Kuznetsov, and P. Mégret, "Refractive index changes in rare earth-doped optical fibers and their applications in all-fiber coherent beam combining," in *Coherent Laser Beam Combining*, edited by A. Brignon (John Wiley & Sons, 2013), Chap. 7, pp. 193–230.

[39] A. W. Snyder, "Asymptotic expressions for eigenfunctions and eigenvalues of a dielectric or optical waveguide," IEEE Trans. Microwave Theory Tech. **17**, 1130 (1969).

[40] R. J. Lang, D. Mehuys, D. F. Welch, and L. Goldberg, "Spontaneous filamentation in broad-area diode laser amplifiers," IEEE J. Quantum Electron. **30**, 685 (1994).